1. Hamid AOUDJEREGBA[1], 2. Ahmed TAHOUR [2]

LSTE Laboratory, University Mustapha Stambouli of Mascara, Algeria (1),
Department of Electrical Engineering, ESSA of Tlemcen, Algeria (2),

doi:10.15199/48.2024.03.32

A Robust Controller based on Backstepping-ADRC for WRSG Based Wind Turbine

Abstract. *In this paper, our objective consists to optimize the energy produced by the wind turbines system (WTSs) equipped on Wonder rotor synchronous generator (WRSG) this machine practical in variables speed system. In the first place, we considered using vector control based on PI type regulator; this control resists less to parametric variations and external disturbances of the machine. To remediate this problem we passed to study and designed two driving systems the first is to give pulses to the PWM-Rectifier connected to the generator side by applied backstepping controller based in Lyapunov laws. And the second system is to give pulses to the PWM-Inverter connected to the grid side by applied a novel robust control approach know as on the Active Disturbance Rejection Controller (ADRC) founded on the supervisor of disturbance by using Extended State Observer(ESO). The simulation outcomes demonstrate the effectiveness of the proposed method, particularly in terms of the power quality delivered*

Streszczenie. *W niniejszym artykule naszym celem jest optymalizacja energii wytwarzanej przez system turbin wiatrowych (WTS) wyposażonych w generator synchroniczny Wonder rotor (WRSG), który jest praktyczną maszyną w systemie zmiennej prędkości. W pierwszej kolejności rozważaliśmy zastosowanie sterowania wektorowego opartego na regulatorze typu PI; ta kontrola jest mniej odporna na zmiany parametryczne i zewnętrzne zakłócenia maszyny. Aby zaradzić temu problemowi, przeszliśmy do badań i zaprojektowaliśmy dwa układy napędowe. Pierwszym z nich jest podawanie impulsów do prostownika PWM podłączonego do strony generatora za pomocą zastosowanego regulatora krokowego opartego na prawach Lapunowa. Drugi system polega na przekazywaniu impulsów do falownika PWM podłączonego do sieci poprzez zastosowanie nowatorskiego, solidnego podejścia do sterowania, znanego jako Active Disturbance Rejection Controller (ADRC), opartego na nadzorcy zakłóceń za pomocą Extended State Observer (ESO).Wyniki symulacji pokazują skuteczność proponowanej metody, szczególnie w zakresie jakości dostarczanej energii (**Solidny sterownik oparty na technologii Backstepping-ADRC dla turbin wiatrowych opartych na WRSG**)*

Keywords: Wind-turbine, Maximum Power Point Tracking (MPPT), Wonder rotor synchronous generator (WRSG), back to back converter, Backstepping, active disturbance rejection control ADRC, phase-locked loop (PLL), Extended State Observer (EOS).
Słowa kluczowe: Turbina wiatrowa, śledzenie punktu mocy maksymalnej (MPPT), generator synchroniczny Wonder rotor (WRSG), konwerter back-to-back, backstepping, aktywna kontrola odrzucania zakłóceń ADRC, pętla fazowa (PLL), Extended State Observer (EOS).

Introduction

Wind energy has gained attention worldwide due to its clean and environmentally friendly characteristics. In recent years, wind energy has shown strong competitiveness in all types of energy, so the installed capacity of wind turbines has been continuously increasing [1] in power generation systems, wound rotor synchronous generators (WRSG) are frequently utilized because of their many benefits, such as their suitability for high power generation, increased power factor, separate control of real and reactive power assets,. It is less sensitive to grid faults because it is electrically isolated from the grid and Gearbox unnecessary [2].

The total energy extracted from a WTS-VS system depends not only on the weather conditions, but also on the applied control. Generally, specialized control algorithms are required to guarantee, in one hand, the extraction of the maximum power and in the other hand the control of active and reactive powers injected into grid [3].

In this paper, the backstopping algorithm have been selected and utilized to extract the maximum power from the WTS-VS due to its robustness and fast tracking response. And for the grid side control, a new robust control strategy based on the Active Disturbance Rejection Controller (ADRC) have been proposed and used to regulate the DC link voltage as well as to control the injection of active and reactive powers into the grid. [4].

The system being studied, as shown in Figure 1, comprises of a horizontal-axis wind turbine with three blades that operates under various wind conditions to convert kinetic energy into mechanical energy. The mechanical energy is then converted into electrical energy by a 1500 KW WRSG. The system also includes two converters (Machine side and Grid side Converters) connected via a DC bus to allow power exchange, and a three-phase RL filter that connects the converters to the electrical grid and reduces the total harmonics distortion of the current.

This paper has been organized in fourth sections where where the first section was for the paper introduction, the second has focalized modelling of the wind energy conversion chain. The third section was devoted to the mathematical model of the backsteping and ADRC controllers. The simulation results of the wind energy conversion system are presented in fourth section.

2. WTS-VS MODELLING

2.1 Wind turbine equivalent model

The basic function of the wind turbine is to intercept and transform the wind's energy into mechanical energy, the turbine power and aerodynamic torque developed are given by the following relation: [5] [6].

(1) $$P_{\text{aero}} = C_p\left(\lambda,\beta\right)\frac{1}{2}\rho\pi R^2 v^3$$

(2) $$T_{aero} = \frac{1}{2\Omega_t} C_p\left(\lambda,\beta\right)\rho s v^3$$

Where ρ is the air density; S is the the surface swept by the blades of the turbine of radius R; v is the wind speed Ω_t is the turbine angular speed.

With:C_P is the power coefficient 'is depends on the turbine characteristics (speed ratio λ and pitch angle β). Its expression is given by equation (3) [5-7].

(3) $$C_P\left(\lambda,\beta\right) = -0.6175\left(\frac{116}{\lambda'} - 0.4\beta - 5\right)e^{\frac{-21}{\lambda'}} + 0.1405\lambda$$

(4) $$\lambda_0 = \frac{1}{0,08\beta+\lambda} - \frac{0,035}{\beta^3+1}$$

(5) $$\lambda = \frac{\Omega_t R}{V}$$

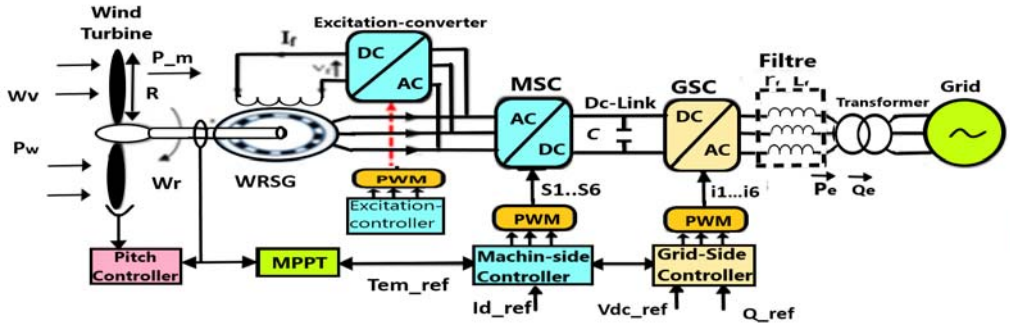

Fig.1. wind turbines system based (WRSG)

The dynamic equation of the synchronous generator is given by : [8]

$$J\frac{d\Omega_t}{dt} = T_{aero} - T_{em} - f\Omega_t \tag{6}$$

Where : J represents the turbine's inertia, Tem is the electromagnetic torque of the electric machine, f is the coefficient of friction

Fig. 2 represents the power coefficient C_P as a function of β and λ While Figure 3 represents the mechanical power as a function of the turbine rotor speed for different values of the wind speed [12]

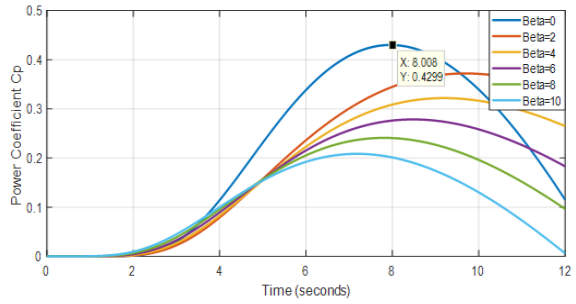

Fig.2. The power coefficient characteristics

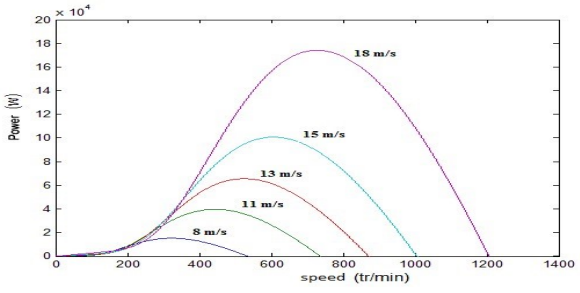

Fig.3. the characteristics of the mechanical power as Function of the turbine speed.

2.2. WRSG generator modelling

The generator chosen for the conversion of wind energy is the synchronous generator [9, 10-11]. The dynamic model of synchronous generator in d-q frame can be represented by the following equations:

$$\begin{cases} v_d = -\left(R_s i_{ds} + L_d \dfrac{di_{ds}}{dt}\right) + L_q \omega_e i_{qs} \\ v_q = -\left(R_s i_{qs} + L_q \dfrac{di_{qs}}{dt}\right) - L_d \omega_e i_{ds} + L_{ff} \omega_e i_f \\ v_f = R_f i_f + L_{ff} \dfrac{di_f}{dt} \end{cases} \tag{7}$$

The electromagnetic torque is given by:

$$T_{em} = \frac{3}{2} P\left[L_{ff} i_f + \left(L_d - L_q\right) i_{sd}\right] i_{sq} \tag{8}$$

Where R_S is the stator resistance, R_f is the rotor resistance, L_d and L_q are the direct and quadrature inductances, L_{ff} is the rotor inductance i_{sd} and i_{sq} are the stator currents, i_f is the excitation current, and P is the pair poles.
w_e is the WRSG speed and it is given by:

$$\omega_e = P\Omega_t \tag{9}$$

2.3. Modelling of The Back to Back Converters

The rectifier (MSC). is used to regulates the generator torque and speed while the inverter (GSC) control the active and reactive power delivery to the grid by the wind energy system. They are both two-level controlled voltage sources converters (VSC) and bidirectional based on IGBT transistors and controlled with the use of the pulse width modulation(PWM). [13-14].
The dq frame voltages are given by:

$$\begin{cases} U_{di} = s_d V_{dc} \\ U_{qi} = s_q V_{dc} \end{cases} \tag{10}$$

With:

$$I_{inv} = s_d i_{dg} + s_q i_{qg} \tag{11}$$

2.4. DC Link and Filter Modelling

DC-link capacitors store energy. Hence, decreasing DC-link capacitance reduces converter cost and volume. However, this reduction capacitance causes considerable voltage fluctuation, which destabilizes the system [15]

The DC Link Voltage can be expressed by:

$$\frac{dV_{dc}}{dt} = \frac{1}{C}\left(i_r - i_i\right) \tag{12}$$

Alternatively, C is the DC link Capacitor.
is the synchronous generator [9, 10-11]. The dynamic model of synchronous generator in d-q frame can be represented by the following equations:

$$\begin{cases} U_{gd} = v_{id} - R_f i_{gd} - L_f \dfrac{di_{gd}}{dt} + L_f \omega_s i_{gq} \\ U_{gq} = v_{iq} - R_f i_{gq} - L_f \dfrac{di_{gq}}{dt} - L_f \omega_s i_{gd} \end{cases} \tag{13}$$

Where, v_{id} , v_{iq} represents the inverter voltage, Ugq, Ugd are the grid voltages and i_{gq},i_{gd} are currents passing through the filter.

3.Control of the wind turbines system (WTSs)

3.1. Control Maximum Power Point Tracking (MPPT)

In order to maximize the amount of power out of the wind turbine, the rotational speed has to be kept at the optimal value of the tip speed ratio, which is denoted by the notation λopt. This causes the turbine to work at its most efficient [16]. The power output that should be optimally achieved from a wind turbine may be expressed as:

(14)

$$P_{m\_opt} = 0.5\rho AC_{p\_opt}\left(\frac{\omega_{m\_opt}R}{\lambda_{opt}}\right)^3 = K_{opt}\left(\omega_{m\_opt}\right)^3$$

Where:

(15)

$$\begin{cases} K_{opt} = 0.5\rho AC_{p\_opt}\left(\dfrac{R}{\lambda_{opt}}\right)^3 \\ \omega_{m\_opt} = \dfrac{\lambda_{opt}}{R}v_w = K_w v_w \end{cases}$$

3.2. Conventionally Vector control:

The basic idea contributes to converting the mathematical model into a linear model by considering (i_{sd_ref} = 0 , i_{sq}=i_s) in which the q-axis loop is for wind turbine speed or torque control and the d-axis loop is for current generator control, The reference signal is obtained as follows from Eq. (8)

(16)

$$\begin{cases} i_{sd\_ref} = 0 \\ i_{sq\_ref} = \dfrac{2}{3P}\dfrac{T_{em\_opt}}{L_{ff}i_f + \left(L_d - L_q\right)i_{sd}} \end{cases}$$

3.3 Backstepping Design for Machine Side Control

The backstepping controller is one of the most important nonlinear control methods [17]. The basic idea of this controller is to find the control equations based on Lyapumov's law of stability, where each step introduces a new reference variable for the next step, One of the most important advantages of this algorithm is that it is not affected by the change of parameters [18].

Step1: Backstepping speed controller

The speed tracking error can be defined by:

(17) $$z_\Omega = \Omega_m^* - \Omega_m$$

The speed error dynamics is written as follows:

(18)

$$\dot{z}_\Omega = \dot{\Omega}_m^* + \frac{3p}{2J}\left(L_q - L_d\right)i_{ds}i_{qs} + \frac{p}{J}M_{sf}i_f i_{qs} + \frac{f}{J}\Omega_m - \frac{T_m}{J}$$

The objective of this first step is to cancel the speed tracking error. We use the Lyapunov function defined by the relation

(19) $$V_\Omega = \frac{1}{2}z_\Omega^2$$

The Lyapunov function derivative is given as:

(20)

$$\dot{V}_\Omega = z_\Omega\left\{\dot{\Omega}_m^* + \frac{p}{J}\left(L_q - L_d\right)i_{ds}i_{qs} + \frac{p}{J}M_{sf}i_f i_{qs} + \frac{f}{J}\Omega_m - \frac{T_m}{J}\right\}$$

To ensure the system stability, a negative value for V_Ω must be chosen. Therefore, the currents $i^*_{\_ds}$ and $i^*_{\_qs}$ are considered as the virtual system inputs. Thus

(21)

$$\begin{cases} i_{ds}^* = 0 \\ i_{qs}^* = \dfrac{J}{pM_{sf}i_f + p\left(L_q - L_d\right)i_{ds}}\left[K_{\Omega m}z_{\Omega m} - \dot{\Omega}_m^* - \dfrac{f}{J}\Omega_m + \dfrac{T_m}{J}\right] \end{cases}$$

Then

(22) $$\dot{V}_\Omega = -k_\Omega z_\Omega^2, \text{ with } k_\Omega > 0$$

Step2: Backstepping current controller

The second step of this algorithm resides on the control voltages calculation v_{qs} and v_{qs} which will be calculated based on the system virtual inputs. The stator currents i_{sd} and i_{sq} which are chosen as virtual inputs will have as errors:

(23)

$$\begin{cases} z_d = i_{ds}^* - i_{ds} \\ z_q = i_{qs}^* - i_{qs} \end{cases}$$

Consider the following Lyapunov candidate function:

(24) $$\dot{z}_\Omega = \frac{1}{J}\left(-K_s J z_\Omega - \frac{3}{2}n_p\varphi_f z_q - \frac{3}{2}n_p\left(L_d - L_q\right)i_q z_d\right)$$

(25)

$$\begin{cases} e_q = \dfrac{1}{2}z_q^2 + \dfrac{1}{2}z_q'^2 \\ e_d = \dfrac{1}{2}z_d^2 + \dfrac{1}{2}z_d'^2 \end{cases}$$

By taking the time derivative of Vq and Vd, and by replacing the suitable terms, The time derivative is computed as :

(26)

$$\dot{V}_q = z_q\left\{\frac{di_{qs}^*}{dt} - \frac{di_{qs}}{dt} + K_q'\left(i_{qs}^* - i_{qs}\right)\right\} + z_q'K_q'\left(i_{qs}^* - i_{qs}\right)$$

$$+z_q'K_q'\left(i_{qs}^* - i_{qs}\right)$$

$$= z_q\left\{\frac{di_{qs}^*}{dt} + \frac{r_s}{L_q}i_{qs} + \omega_e\frac{L_d}{L_q}i_{ds} - \omega_e\frac{M_{sf}}{L_q}i_f + \frac{1}{L_q}v_{qs} + K_q'\left(i_{qs}^* - i_{qs}\right)\right\}$$

27)

$$\dot{V}_d = z_d\left[\frac{di_{ds}^*}{dt} - \frac{di_{ds}}{dt} + K_d'\left(i_{ds}^* - i_{ds}\right)\right] + z_d'K_d'\left(i_{ds}^* - i_{ds}\right)$$

$$= z_d\left[\frac{r_s}{L_d}i_{ds} - \omega_e\frac{L_q}{L_d}i_{qs} - \frac{M_{sf}}{L_d}\frac{di_f}{dt} + \frac{v_{ds}}{L_d}\right] + \left(z_d + z_d'\right)K_d'\left(z_d - z_d'\right)$$

In order to ensure a system stability one must choose the constants K_d and K_q of the positive constants. On the other hand, the Lyapunov function derivative will be negative if we impose as reference voltages:

(28)

$$\begin{cases} v_{qs} = -K_q L_q z_q - L_q \dfrac{di_{qs}^*}{dt} - r_s i_{qs} - \omega_e L_d i_{ds} + \omega_e M_{sf} i_f \\ v_{ds} = -K_d L_d z_d - r_s i_{ds} + \omega_e L_q i_{qs} + M_{sf} \dfrac{di_f}{dt} \end{cases}$$

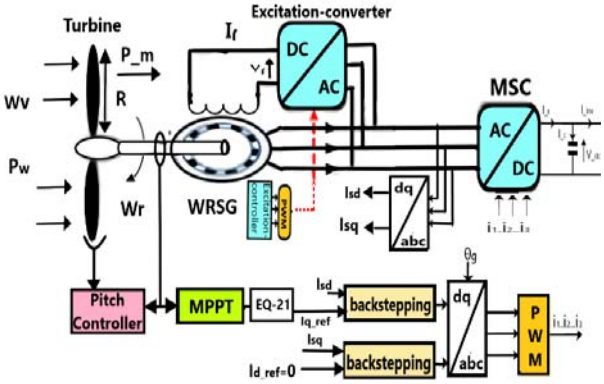

Fig.4. Backstepping approach for MSC

3.4. Control of the Grid Side Converter by LADRC

The GSC is connected to the grid by an intermediary line characterized by a resistance Rf and an inductance Lf. we present ADRC control strategies to stabilize the dc-link voltage and to adjust the active and reactive power delivery into the grid during weather variations to achieve unity power factor as shown in Fig 5 The phase locked loop (PLL) is used for the detection of the grid voltage magnitude the angle θg by orientation of the q-axis voltage to zero, this ensures the synchronization of the system with the electrical power grid [19].

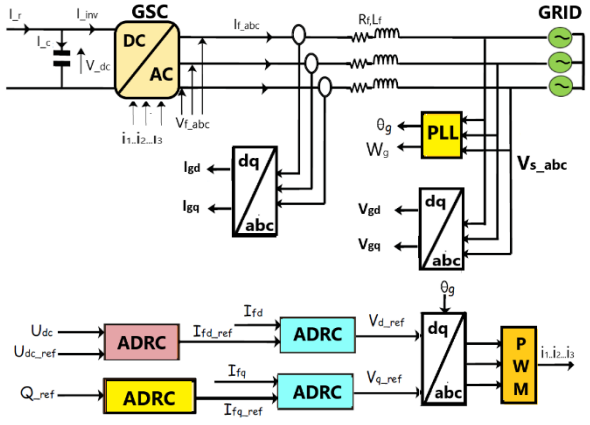

Fig.5. Grid side converter control by ADRC

3.5. Mathematical Model of ADRC

ADRC is robust control strategy proposed by Jingqing Han in 2009 [20]. Te main advantage of this control is to estimate and compensate in real time the various external and internal disturbances of the system, without having a detailed model of the system only utilizing the data about its inputs and outputs [21]. To ensure that, the controller contains three blocks: differentiator trackers (DT), feedback controller (FC), and extended state observer (ESO). It involves also an inner loop to reject the total disturbance and an outer one to deliver the desired signal the applied ADRC method design is shown in fig.6.

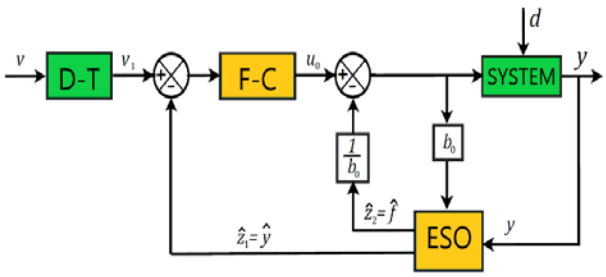

Fig.6. Grid side converter control by ADRC

where, v is the input signal, v1 is the input tracking signal; y is the system feedback signal; z1 is the estimated tracking signal; z2 is the total disturbances estimation; b0 is the compensation factor; z2=b0 is the internal and external disturbances compensation; u0 is the initial control object by NLSEF; u is the final control signal after disturbance compensate.

For a first-order controlled object, its mathematical model of ADRC is set as [22]

Step 1: defined the mathematical model of the TD

(29)
$$\begin{cases} \varepsilon_0 = v_1 - v, \\ \dfrac{dv_1}{dt} = -rfal\left(\varepsilon_0, \alpha_0, \delta_0\right) \end{cases}$$

Step 2: the model of ESO

(30)
$$\begin{cases} \varepsilon = z_1 - y \\ \dfrac{dz_1}{dt} = z_1 - \beta_{01} fal\left(\varepsilon, \alpha, \delta\right) + bu\left(t\right), \\ \dfrac{dz_2}{dt} = \beta_{02} fal\left(\varepsilon, \alpha, \delta\right) \end{cases}$$

Step 3: feedback FC block it is represented

(31)
$$\begin{cases} \varepsilon_1 = v_1 - z_1 \\ u_0 = \beta_1 fal\left(\varepsilon_1, \alpha_1, \delta_1\right), \\ u = u_0 - \dfrac{z_2}{b_0}, \end{cases}$$

Step 4: the total disturbance (internal and external)

(32)
$$f\left(\varepsilon, \alpha, \delta\right) = \begin{cases} |\varepsilon|^{\alpha} \, sgn\left(\varepsilon\right), & |\varepsilon| > \delta \\ \dfrac{\varepsilon}{\delta^1 - \alpha}, & |\varepsilon| \le \delta \end{cases}$$

where β_{01}, β_{02}, β_{03} are output error factors, δ is the filtering factor to ESO and α is a nonlinear factor.

the active and reactive powers are then given by

(33)
$$\begin{cases} P_g = \dfrac{3}{2} v_{gd} i_{fd} \\ Q_g = -\dfrac{3}{2} v_{gd} i_{fq} \end{cases}$$

Is shows that the active and reactive powers will be controlled, respectively, by currents i_{fd} and i_{fq}.

3.6. DC Bus Voltage Control by L'ADRC

The power flowed in the DC bus as shown in are thus expressed

$$P_{dc} = U_{DC} C \frac{dU_{DC}}{dt} = U_{DC} \left(i_r - i_i \right) \tag{34}$$

When the losses in the RL filter, the capacitor and in the two power converters are neglected, the powers across the DC bus are expressed by

$$P_{\mathrm{dc}} = P_{MSC} - P_{GSC} \tag{35}$$

Where, P_{dc} is the power absorbed by the capacitor, P_{MSC} the power delivered by the MSC, and P_{GSC} the power absorbed by the GSC [23]. Negative values mean that the devices are generating power.

By taking into account Eq.35-34 the DC bus voltage can be expressed by:

$$CU_{dc} \frac{dU_{dc}}{dt} = U_{dc} \left(i_r \right) - \frac{3}{2} v_{gd} i_{fd}$$

or

$$\frac{dU_{dc}^2}{dt} = \frac{2U_{dc}}{C} \left(i_r \right) - \frac{3v_{gd}}{C} i_{fd} \tag{36}$$

And we put:

$$Z = U_{dc}^2$$

$$\frac{dZ}{dt} = \frac{2\sqrt{Z}}{C} \left(i_{\mathrm{r}} \right) - \frac{3v_{gd}}{C} i_{fd} \tag{37}$$

So we obtain:

$$\begin{cases} f\left(y, d, t\right) = \dfrac{2\sqrt{z}}{C} \left(i_{\mathrm{r}} \right) \\ b_0 = -\dfrac{3v_{gd}}{C} \\ u = i_{fd} \end{cases} \tag{38}$$

3.7. Control of Filter Currents by L'ADRC

The external voltage regulation loop makes it possible to maintain the voltage across the capacitor Udc and to generate the current reference i for the internal current loop. For the current i_{fq_ref}, it is calculated by the desired delivery of reactive power:

$$i_{fq-ref} = -\frac{2}{3v_{gd}} Q_{f-ref} \tag{39}$$

The filter currents are given in canonical form of ADRC

$$\frac{di_{fd}}{dt} = \frac{1}{L_f} \left(-R_f i_{fd} - v_{gd} + L_f \omega_g i_{fq} \right) + \frac{v_{fd}}{L_f} \tag{40}$$

Whith:

$$\begin{cases} f\left(y, d, t\right) = \dfrac{1}{L_f} \left(-R_f i_{fd} - v_{gd} + L_f \omega_g i_{fq} \right) \\ b_0 = \dfrac{1}{L_f} \\ u = v_{fd} \end{cases} \tag{41}$$

For q-axis current:

$$\frac{di_{fq}}{dt} = \frac{1}{L_f} \left(-R_f i_{fq} - L_f \omega_g i_{fd} \right) + \frac{v_{fq}}{L_f}. \tag{42}$$

With:

$$\begin{cases} f\left(y, q, t\right) = \dfrac{1}{L_f} \left(-R_f i_{fq} - L_f \omega_g i_{fd} \right) \\ b_0 = \dfrac{1}{L_f} \\ u = v_{fq} \end{cases} \tag{43}$$

4. Results and Discussion

The simulation was executed using MATLAB/Simulink software and the performances of the control strategies are studied and compared in this work. To exanimate the tracking effectiveness of the proposed control, a variable wind speed profile is applied as shown in Fig.6. The simulation. Parameters are given in Appendix. A

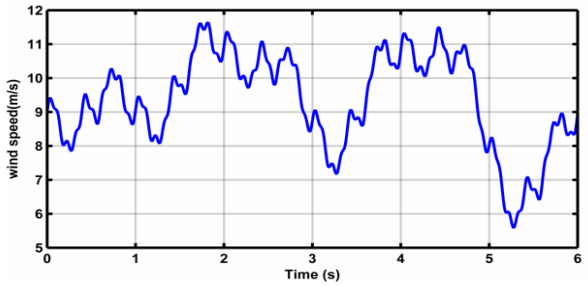

Fig.7. The applied random wind speed profile

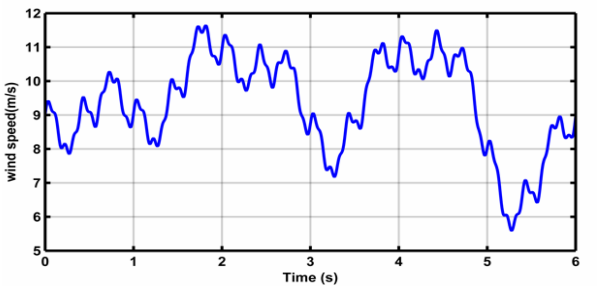

Fig.8. WRIG rotational speed

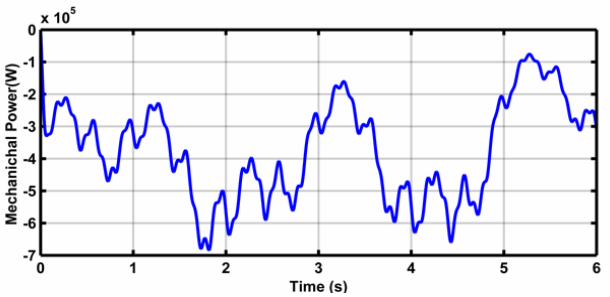

Fig.9. The captured mechanical power

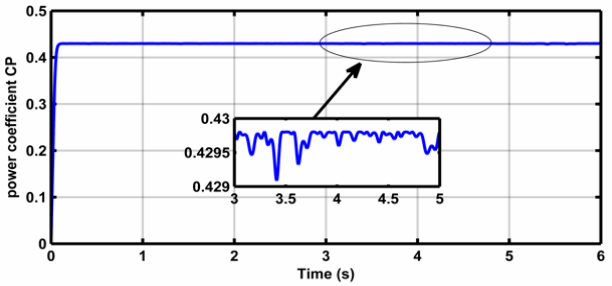

Fig.10. The Power coefficient *Cp*

As can be noticed in Fig. 9, the power coefficient has been maintained at its optimal value (*Cp_max* = 0:43) which shows the effectiveness of the MPPT strategy in terms of maximum power extraction.

Figures 10-11 present the simulation results of the stator side converter, for the two control strategies (backstepping control and PI control).

As it can be seen in Figures 10 and 11, where the direct axis current Id and quadrature current Iq the control by PI and the control by backstepping tracks their references, but the control by backstepping is faster. The generated currents are shown in Fig 12

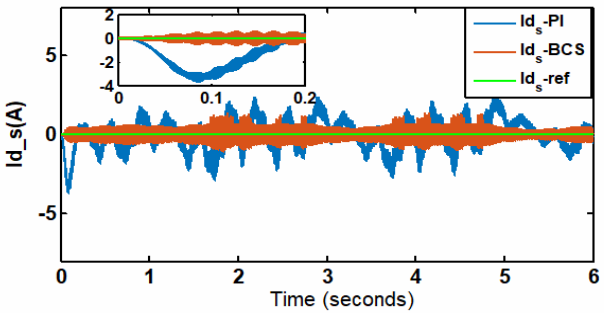

Fig.11. The control of the stator current Isd by backstepping and PI

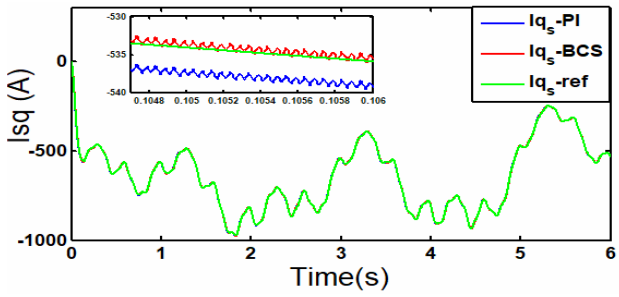

Fig.12. The control of the stator current *Isq* by backstepping and PI

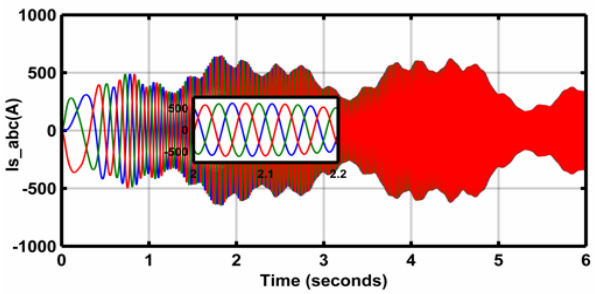

Fig.13. WRSG Stator Currents Isabc

As illustrated in Figures 15, the Linear-ADRC approach offers a faster trackness characteristic while controlling the DC-Link Voltage compared to the conventional approach by PI, where the DC-Link Voltage is maintained at its reference without presenting an overshoot at the transition all regime with some fluctuations which are due to the stochastic nature of wind speed. Also, it can be noticed that the Linear-ADRC regulates the grid currents to their references.

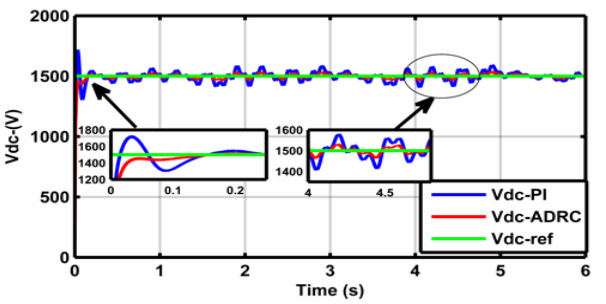

Fig.14. the control of the DC Bus Voltage Vdc by ADRC and PI

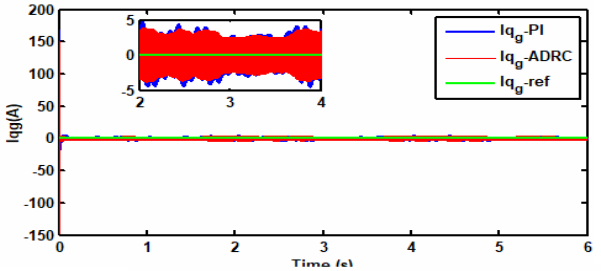

Fig.15. the control of the grid current Igq by ADRC and PI

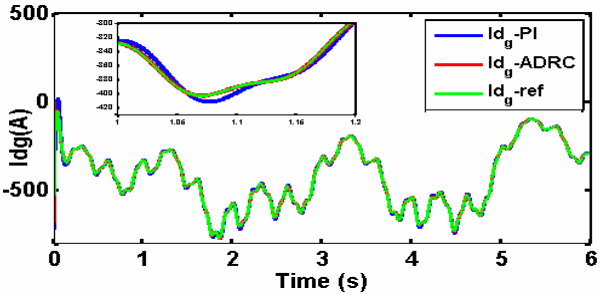

Fig.16. the control of the grid current *Igd* by ADRC and PI

The regulation of both active and reactive powers is also performed. As can be seen in Figure 16, the power injected into the grid tracks its reference (the extracted power from the wind turbine minus joules and DC-Link losses). And the reactive power was set to zero to ensure a unit power factor. Hence the voltage and current of the grid are in phase as seen in Figure 16.

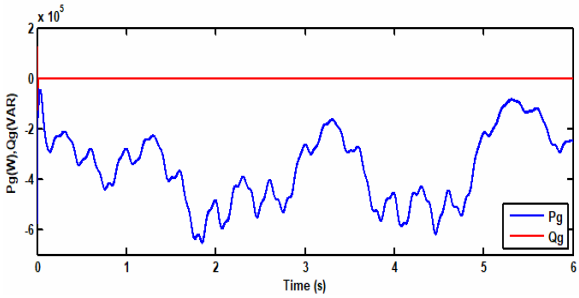

Fig.17. the injected active and reactive powers to the grid

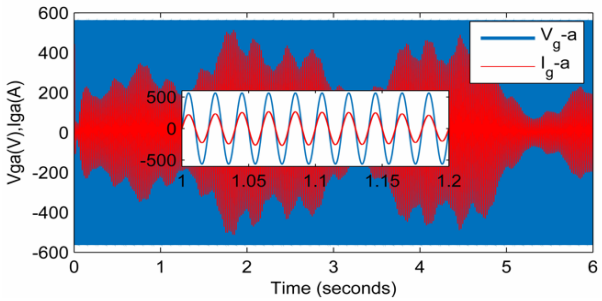

Fig.18. the injected active and reactive powers to the grid

4.1. Simulation Results Under Parametric Variation

In order to test the robustness of the proposed control strategies, we have performed a change in the internal parameter of the WRSG, the stator inductance Ls by an increase of 50%, of their nominal value. The results obtained by LADRC are compared with the classical PI controller. The utilized wind speed profile is given in Fig 18.

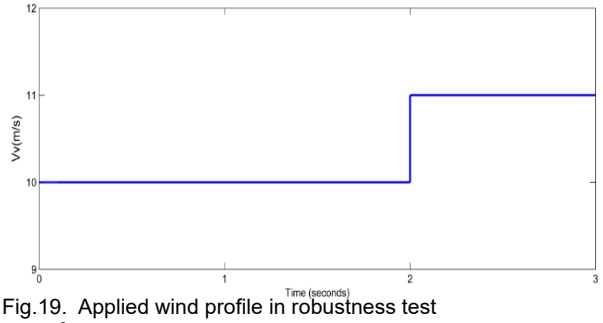

Fig.19. Applied wind profile in robustness test

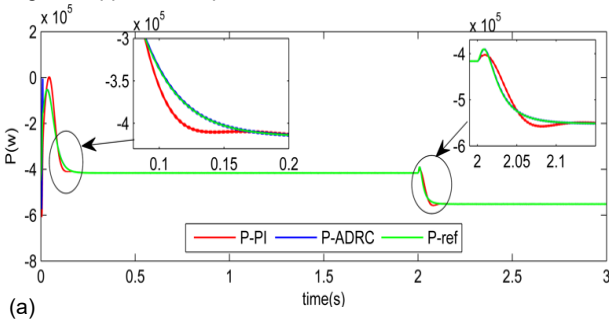

(a)

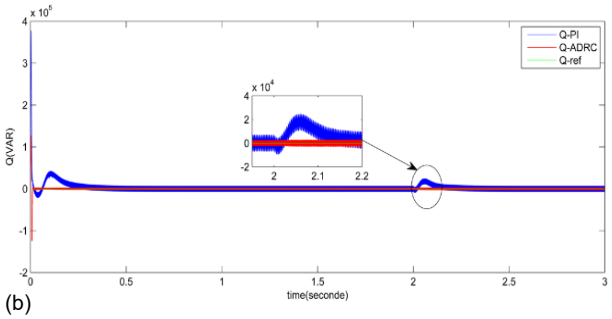

(b)

Fig.20. (a) (b) Active and Reactive power of PI whith ADRC

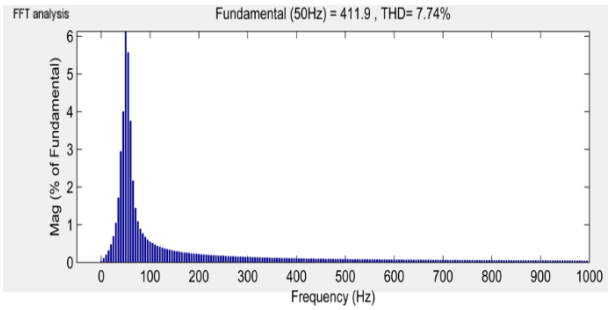

(a) Conventionnelle control (PI)

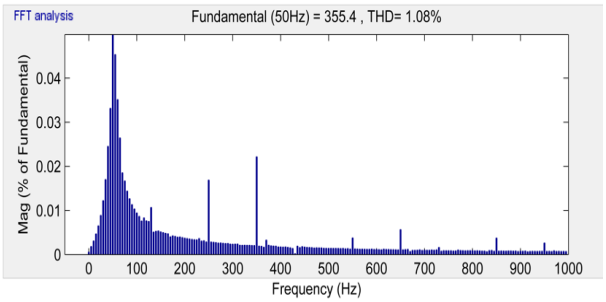

(b) ADRC control

Fig.21. Grid current FFT analysis (a) Conventionnelle control (PI) , (b) ADRC control.

The results of the spectral analysis for the grid phase current shown in Figure 21 shows that the ADRC control guarantees a better waveform quality of the grid current.

5. Conclusion

In this study, we focus on the modelling and regulation of a wonder rotor synchronous generator-based wind energy conversion system. In order to optimize the dynamical performance, robustness of the entire system against the intermittent nature of wind velocity and to extract the maximum power from the wind energy delivers it to utility power grid. We developed and presented a comparative study of the two strategies PI and combination between two controllers backstopping-ADRC The goal is to control the generator's electromagnetic torque (MPPT), Regulating the DC bus voltage and grid currents to their references controlled active and reactive powers.

The simulation results demonstrate that the suggested control strategy is efficient in terms of fast tracking and robustness to parameter sensitivity compared to the conventional PI controller.

Appendix

WRSM Wind Turbine Parameters :

• Radius: R = 24 m • Nominal wind speed: Vv = 12 m·s-1 • Total inertia of the mechanical transmission: JT = 10kg·m2,

• CP max = 0:48, • $\lambda_{optimal} = 8$,1,
• Stator resistance: $R_s = 0.022\ \Omega$ • Stator inductance: Ld=12.18e-3 mH Lq=8.53e-3 mH • Pair poles: $P = 30$ • DC bus voltage: $V_{dc} = 1500$ V • DC bus Capacitor: $C = 5000 \cdot 10\text{-}6$ F • Filter Resistance: $R_f = 0.1\ \Omega$ • Filter Inductance: $L_f = 2\ 10\text{-}3$ H

Authors: *Phd. AOUDJEREGBA HAMID University Mustapha Stambouli of Mascara, Algeria*
Pr. Tahour Ahmed, School of Applied Sciences Tlemcen.
E-mails: aoudj.hamid@univ-mascara.dz
E-mails: tahourahmed@yahoo.fr

REFERENCES

[1] B.K. Sahu, Wind energy developments and policies in China: A short review, Renew. Sustain. Energy Rev. 81 (2018) 1393–1405.
[2] Gupta, A., Bhushan, H., Samuel, P. "Generator Topologies with Power Electronics Converters for a Wind Energy Conversion System", A Review
[3] AHMAD, Zameer and SINGH, S. N. Modeling and Control of Grid Connected Photovoltaic System-A Review. International Journal of Emerging Technology and Advanced Engineering, 2013, vol. 3, no 3, p. 2250-2459.
[4] HAN, Jingqing. From PID to active disturbance rejection control. IEEE transactions on Industrial Electronics, 2009, vol. 56, no 3, p. 900-906.

[5] C. Mohssine, ‘A Comparative Study of PI, RST and ADRC Control Strategies of a Doubly Fed Induction Generator Based Wind Energy Conversion System’, International Journal of Renewable Energy Research (IJRER), vol. 8, no. 2, Art. no. 2, Jun. 2018
[6] A. Jabal Laafou, A. Ait Madi, A. Addaim, and A. Intidam, ‘Dynamic Modeling and Improved Control of a Grid-Connected DFIG Used in Wind Energy Conversion Systems’, Mathematical Problems in Engineering, vol. 2020, p. e1651648, Jul. 2020,
[7] X. Yin and X. Zhao, ‘Optimal power extraction of a two-stage tidal turbine system based on backstepping disturbance rejection control’, International Journal of Electrical Power & Energy Systems, vol. 132, p. 107158, Nov. 2021,
[8] Mi, C., Filippa, M., Shen, J., Natarajan, N: Modeling and Control of Variable Speed Constant Frequency Synchronous Generator With brushless Exciter. IEEE Transactions on Industry Application 40(2), 565–573 (2004)
[9] Mi, C., Filippa, M., Shen, J., Natarajan, N.: Modeling and Control of Variable Speed Constant Frequency Synchronous Generator With brushless Exciter. IEEE Transactions on Industry Application 40(2), 565–573 (2004)
[10] Refoufi, L., Al Zahawi, B.A.T., Jack, A.G.: Analysis and modelling of the steady state behavior of the static Kramer induction generator. IEEE Transactions on Energy Conversion 14(3), 333–339 (1999)
[11] El Aimani, S.: Modélisation de différentes technologies d’éoliennes intégrées dans un réseau de moyenne tension. Thèse de doctorat de l’Ecole Centrale de Lille (ECL) Cohabilité avec L’université des sciences et technologies de Lille 1 (USTL), December 06 (2004)
[12] S.R. Guda, ‘Modeling and Power Management of a Hybrid Wind-Microturbine Power Generation’, Master thesis, University of Bozeman, Monata, Juillet 2005.
[13] Tahir, A., Mohamed, E. M., Abdulhafid, E. F., & Mohamed, F. (2020). Grid connected wind energy system through a back-to-back converter. Computers&Electrical Engineering, 85, 106660.
[14] MALINOWSKI M., 2001-"Sensorless Control Strategies for Three-Phase PWM Rectifiers", Warsaw, Poland, 18-25
[15] YIN L.; ZAHO Z.; LU T.; YANG SH.; ZOU G.,2014-"An Improved DC-Link Voltage Fast Control Scheme for a PWM Rectifier-Inverter System", IEEE TRAN, on IA, 50(1), 462-473.
[16] Md. Enamul Haque, Michael Negnevitsky and Kashem M. Muttaqi, “A Novel Control Strategy for a Variable-Speed Wind Turbine With a Permanent-Magnet Synchronous Generator,” IEEE Transactions On Industrty Applications,Vol. 46, No. 1, pp. 331-339, Jannuary/February 2010.
[17] JEON B J.; SEO M G.; SHIN H S.; TSOURDOS A.,2020-"Understandings of Classical and Incremental Backstepping Controllers with Model Uncertainties", IEEE TRAN, on ES, 56(4), 2628-2641
[18] RAHMAN M A.; VILATHGAMUMA M.; NASIR ULDIN M.; TSENG K T.,2003-" Nonlinear Control of Interior Permanent-Magnet Synchronous Motor", IEEE TRAN, on IA, 39(2), 408-416.
[19] LIU, Baoquan, ZHUO, Fang, ZHU, Yixin, and al.A three-phase PLL algorithm based on signal reforming under distorted grid conditions. IEEE Transactions on Power Electronics, 2015, vol. 30, no 9, p. 5272- 5283
[20] HAN, Jingqing. From PID to active disturbance rejection control. IEEE transactions on Industrial Electronics, 2009, vol. 56, no 3, p. 900-906
[21] S. Yi Huang, W. Zhang, ’’Development of active disturbance rejection controller’’, Control Theory & Applications, Vol. 19, pp 485-492, 2005.
[21] HERBST, Gernot. A simulative study on active disturbance rejection control (ADRC) as a control tool for practitioners. Electronics, 2013, vol. 2, no 3, p. 246-279.